A comparison of antenna placement criteria based on the Cramér–Rao and Barankin bounds for radio interferometer arrays

Jianhua Wang, Lucien Bacharach, Pascal Larzabal, Mohammed Nabil El Korso

A comparison of antenna placement criteria based on the Cramér-Rao and Barankin bounds for radio interferometer arrays⋆

Jianhua Wang[a], Lucien Bacharach[a,*], Pascal Larzabal[a], Mohammed Nabil El Korso[b]

[a] *Université Paris-Saclay, SATIE, 4, avenue des Sciences, Gif-sur-Yvette, 91190, France*
[b] *Université Paris-Saclay, L2S, 3, rue Joliot-Curie, Gif-sur-Yvette, 91190, France*

Abstract

In this paper, we consider the problem of antenna placement for radio interferometer arrays. In this type of applications, signal-to-noise ratios (SNR) are typically low, and possibly lower than a SNR threshold under which the estimation performance of source parameters may degrade significantly. In this regime, the Cramér-Rao bound (CRB), which is often used for array design, is not a tight bound of the MSE. Therefore, we study the use of a Barankin-type bound (BTB) as an alternative array design criterion. We assess and compare the array geometries based on the CRB and the BTB in terms of MSE for a source's DOA and intensity. We also study how both geometries perform for imaging purposes. Specifically, the obtained results are assessed in terms of *uv*-plane coverage (completeness of spatial frequency sampling), mainlobe width and sidelobe level of the synthesized beam, as well as image reconstruction performance. Numerical experiments show that the BTB-based design leads to better overall estimation performance over a fairly wide range of SNR and to an enhanced array imaging capability, compared with a CRB-based approach.

Keywords: Antenna placement, Barankin bound, Cramér-Rao bound

1. Introduction

In recent decades, radio interferometer arrays have grown in size, with many more antenna elements and much wider spatial spread. The increased number of antennas improves resolution and sensitivity, as is the case of modern instruments, such as LOFAR [1] or SKA [2, 3]. Since their accuracy highly depends on the antenna locations, antenna placement makes up a critical task in the design phase of the instruments.

In radio interferometry, the data used to construct sky images correspond to the signal correlations between each pair of antennas, also referred to as *visibilities*. Due to the Fourier transform relationship between the visibilities and the sky image [4], a fundamental characteristic of radio interferometers is the sampling function of the visibilities in the spatial frequency domain, generally referred to as *uv*-plane coverage in radio astronomy. Each visibility is associated with a baseline vector that connects the corresponding pair of antennas. The collection of the array baseline vectors, projected on the plane orthogonal to the reference direction (generally the center of the desired image), forms the *uv*-plane coverage. Consequently, classical approaches for radio interferometer design consist in placing antennas so as to obtain a desired *uv*-plane sampling function, or equivalently a desired point-spread function in the image domain (typically, with a narrow main lobe and low sidelobes) [5, 6].

The *uv*-plane coverage plays a key role when considering imaging methods based on beamforming. If model-based, parametric techniques such as maximum likelihood estimation are used [7], it seems more appropriate to formulate array design criteria based on the statistical performance of such methods, which is usually assessed in terms of mean-squared error (MSE). Assessing the MSE of an estimator requires numerous Monte-Carlo simulations, which can quickly become computationally intensive, and sometimes unfeasible, as the number of unknown parameters increases. This is especially burdensome if MSE is to be used as the cost function to design a system. To overcome this difficulty,

⋆This work was funded in part by the Chinese Scholarship Council (CSC) and by the Farman Institute (PARAISO project).

*Corresponding author.
Email addresses: jianhua.wang@ens-paris-saclay.fr (Jianhua Wang), lucien.bacharach@universite-paris-saclay.fr (Lucien Bacharach), pascal.larzabal@universite-paris-saclay.fr (Pascal Larzabal), mohammed.nabil.el-korso@centralesupelec.fr (Mohammed Nabil El Korso)

lower bounds of the MSE can be used as performance indicator, such as the Cramér-Rao bound (CRB). In addition these bounds have the appealing property of being valid for a family of estimators (namely, unbiased estimators in the case of the CRB, for instance). In array processing, the CRB is commonly used as a design criterion to solve the problem of optimal antenna placement [8, 9], due to its simplicity and existence of closed form. However, it is well-known that the CRB is generally only asymptotically attained, i.e., for a large number of observations and/or high SNR. In nonlinear estimation problems, a threshold SNR exists, under which the MSE significantly deviates from the CRB. For low SNR, the CRB is consequently not appropriate to describe estimation performance. Numerous other bounds have been proposed in the literature, which can be used to predict the SNR threshold (see e.g., [10, 11] for an overview). Among them, Barankin-type bounds (BTB), such as the Hammersley-Chapman-Robbins bound [12], offer a practical way for computing the original Barankin bound [13]. These bounds have been extensively studied in the literature, especially in the field of array processing (see [14–16], for instance). To the best of our knowledge, BTBs have rarely been used to solve an antenna selection problem at low SNR. In [17], the authors used the Bobrovsky-Zakai bound, which can be seen as the Bayesian counterpart of BTBs, in a context of cognitive antenna selection for automotive radar.

Here, we investigate the antenna placement problem by seeking to minimize MSE lower bounds on the parameters of a single source, such as direction of arrival (DOA) and source power. We aim at studying to which extent this relaxed model may lead to relevant array geometries for imaging purposes in radio astronomy. Specifically, we compare antenna placement approaches based on the minimization of the CRB and the BTB, respectively. The performance of both approaches is compared in terms of array beampattern (or dirty beam), baseline diversity, and parameter estimation accuracy. It is shown that a BTB-based design criterion is more suitable than a CRB-based criterion, especially in the SNR transition regime.

The rest of the paper is organized as follows: Section 2 describes the data model and provides some background on MSE lower bounds, Section 3 formulates the optimization problem for antenna placement, and Section 4 presents numerical results and analyses. Finally, conclusions are drawn in Section 5.

2. Data model and associated error lower bounds

2.1. Model formulation

We consider an antenna array consisting of P antennas placed on the Earth's surface, whose location vectors are denoted by $\boldsymbol{\xi}_p = [x_p, y_p, z_p]^\mathsf{T}$, $p = 1, \ldots, P$, in a local coordinate system where the x-axis is oriented towards east of the reference observation point (chosen as the origin), the y-axis is oriented towards north, and the z-axis points at the zenith. We assume the presence of a single, narrowband, far-field source signal $s(t)$, that is zero-mean, complex Gaussian, with an unknown variance denoted by $S = \mathrm{E}\left|s^2(t)\right|$ that corresponds to the source intensity. We are interested in recovering this source intensity, as well as its DOA, which is described by a unit vector $\boldsymbol{\ell} = [l, m, \sqrt{1 - l^2 - m^2}]^\mathsf{T}$, with l and m the direction cosines. The antennas give rise to an independent, identically distributed (i.i.d.) additive noise vector $\mathbf{n}(t) \in \mathbb{C}^P$ that is assumed to be complex Gaussian with covariance matrix $\sigma^2\mathbf{I}$, and uncorrelated with the source signal $s(t)$. In these conditions, noting as $y_p(t)$ the signal received at the p-th antenna, the array signal vector $\mathbf{y}_n = [y_1(t_n), \ldots, y_P(t_n)]^\mathsf{T}$ at sampling time t_n, $n = 0, \ldots, N-1$, can be expressed as

$$\mathbf{y}_n = \mathbf{a}(\boldsymbol{\ell})\, s_n + \mathbf{n}_n, \tag{1}$$

where $\mathbf{a}(\boldsymbol{\ell}) = \left[e^{-\mathrm{j}\frac{2\pi}{\lambda}\boldsymbol{\xi}_1^\mathsf{T}\boldsymbol{\ell}}, \ldots, e^{-\mathrm{j}\frac{2\pi}{\lambda}\boldsymbol{\xi}_P^\mathsf{T}\boldsymbol{\ell}}\right]^\mathsf{T} \in \mathbb{C}^P$ denotes the array response vector (the exponential function is applied element-wise), $\boldsymbol{\Xi} = [\boldsymbol{\xi}_1, \ldots, \boldsymbol{\xi}_P]$ is the $3 \times P$ matrix stacking the antenna coordinates, $s_n = s(t_n)$ and $\mathbf{n}_n = \mathbf{n}(t_n)$. Given the assumptions made about the source and noise signals, the array signal vector $\mathbf{y}_n$ follows a zero-mean, complex Gaussian distribution with covariance matrix

$$\mathbf{R}(\boldsymbol{\theta}) = S\, \mathbf{a}(\boldsymbol{\ell})\, \mathbf{a}^\mathsf{H}(\boldsymbol{\ell}) + \sigma^2\mathbf{I}, \tag{2}$$

where $\boldsymbol{\theta} = [l, m, S, \sigma^2]^\mathsf{T}$ denotes the unknown parameter vector. The likelihood function, for an observation $\mathbf{Y} = [\mathbf{y}_0, \ldots, \mathbf{y}_{N-1}]$ over N independent samples, is given by

$$p(\mathbf{Y}\,;\boldsymbol{\theta}) = \frac{1}{\pi^{NP}|\mathbf{R}(\boldsymbol{\theta})|^N} \exp\left(-\sum_{n=0}^{N-1} \mathbf{y}_n^\mathsf{H}\mathbf{R}^{-1}(\boldsymbol{\theta})\, \mathbf{y}_n\right) \tag{3}$$

where $|\cdot|$ denotes the determinant of its argument.

In this paper, we aim at finding antenna locations $\mathbf{z}_1, \ldots, \mathbf{z}_p$ that lead to minimal MSE on parameter vector $\boldsymbol{\theta}$. We do so by resorting to lower bounds of the MSE, which are described in the next sections.

2.2. Lower bounds of the MSE

The Cramér-Rao and Barankin-type bounds are lower bounds of the MSE for unbiased estimators, which can be shown to satisfy the following matrix inequalities (in the sense that the difference between the left-hand side and the right-hand side is a nonnegative-definite matrix) [10]:

$$\mathbf{C_e} \geq \mathbf{C_B} \geq \mathbf{C_{CR}} \tag{4}$$

where $\mathbf{C_e} = \mathrm{E}[(\widehat{\boldsymbol{\theta}}(\mathbf{Y}) - \boldsymbol{\theta}_0)(\widehat{\boldsymbol{\theta}}(\mathbf{Y}) - \boldsymbol{\theta}_0)^\mathsf{T}]$ is the MSE matrix, $\mathbf{C_{CR}}$ is the CRB and $\mathbf{C_B}$ is a BTB. The CRB is known to be the inverse of the Fisher information matrix (FIM) $\mathbf{F} = \mathrm{E}\Big[\frac{\partial \log p(\mathbf{Y};\boldsymbol{\theta})}{\partial \boldsymbol{\theta}} \frac{\partial \log p(\mathbf{Y};\boldsymbol{\theta})}{\partial \boldsymbol{\theta}^\mathsf{T}}\Big]$, where derivatives are evaluated at the true parameter vector $\boldsymbol{\theta}_0$, that is $\mathbf{C_{CR}} = \mathbf{F}^{-1}$. Barankin-type bounds can be expressed in various ways (see [10] for several examples). In this paper, we investigate the so-called Hammersley-Chapman-Robbins bound [12], which holds for estimators which are unbiased at a number K of test points denoted by $\boldsymbol{\theta}_k$, $k = 1, \ldots, K$. This bound is given by

$$\mathbf{C_B} = \mathbf{H}\left(\mathbf{B} - \mathbf{1}\mathbf{1}^\mathsf{T}\right)^{-1}\mathbf{H}^\mathsf{T} \tag{5}$$

where $\mathbf{H} = [\boldsymbol{\theta}_1 - \boldsymbol{\theta}_0, \ldots, \boldsymbol{\theta}_K - \boldsymbol{\theta}_0]$, and $\mathbf{B}$ is the $(K \times K)$ Barankin matrix whose (i, j)-th component is given by

$$B_{ij} = \mathrm{E}\left[\frac{p(\mathbf{Y}\,;\boldsymbol{\theta}_i)}{p(\mathbf{Y}\,;\boldsymbol{\theta}_0)} \frac{p(\mathbf{Y}\,;\boldsymbol{\theta}_j)}{p(\mathbf{Y}\,;\boldsymbol{\theta}_0)}\right]. \tag{6}$$

2.2.1. Cramér-Rao lower bound

The CRB for the (unconditional) signal model (1) has been well studied in the array processing literature [18–20]. The expression of the FIM results from the Slepian-Bangs formula, which leads to [19]

$$\mathbf{F} = N\left(\frac{\partial \operatorname{vec}\mathbf{R}}{\partial \boldsymbol{\theta}^\mathsf{T}}\right)^\mathsf{H} (\mathbf{R}^{-\mathsf{T}} \otimes \mathbf{R}^{-1}) \frac{\partial \operatorname{vec}\mathbf{R}}{\partial \boldsymbol{\theta}^\mathsf{T}}, \tag{7}$$

where $\otimes$ denotes the Krönecker product, and $\operatorname{vec}(\cdot)$ represents the vectorization operator. The vectorized covariance matrix $\operatorname{vec}\mathbf{R}$ can be written (after dropping the dependence of the array response vector $\mathbf{a}$ on $\boldsymbol{\ell}$ for simplicity) as

$$\operatorname{vec}\mathbf{R} = S\,(\mathbf{a}^* \otimes \mathbf{a}) + \sigma^2 \operatorname{vec}\mathbf{I}, \tag{8}$$

where $(\cdot)^*$ denotes complex conjugation. The derivatives of $\operatorname{vec}\mathbf{R}$ can subsequently be computed as [21]

$$\frac{\partial \operatorname{vec}\mathbf{R}}{\partial l} = -\mathrm{j}\frac{2\pi}{\lambda} S\,(\operatorname{diag}\operatorname{vec}\boldsymbol{\Delta}_x)\,(\mathbf{a}^* \otimes \mathbf{a}) \tag{9}$$

$$\frac{\partial \operatorname{vec}\mathbf{R}}{\partial m} = -\mathrm{j}\frac{2\pi}{\lambda} S\,(\operatorname{diag}\operatorname{vec}\boldsymbol{\Delta}_y)\,(\mathbf{a}^* \otimes \mathbf{a}) \tag{10}$$

where $\boldsymbol{\Delta}_x$ and $\boldsymbol{\Delta}_y$ are $(P \times P)$ matrices whose elements are respectively given by $(\Delta_x)_{ij} = x_i - x_j - \frac{l(z_i - z_j)}{\sqrt{1-l^2-m^2}}$ and $(\Delta_y)_{ij} = y_i - y_j - \frac{m(z_i - z_j)}{\sqrt{1-l^2-m^2}}$, $i, j = 1, \ldots, P$, the $\operatorname{diag}(\cdot)$ operator converts its vector argument to a diagonal matrix with the elements of the vector on the diagonal, and finally

$$\frac{\partial \operatorname{vec}\mathbf{R}}{\partial S} = \mathbf{a}^* \otimes \mathbf{a} \quad \text{and} \quad \frac{\partial \operatorname{vec}\mathbf{R}}{\partial \sigma^2} = \operatorname{vec}\mathbf{I}. \tag{11}$$

It can be noted that expressions (9) and (10) provided here are rewritten from those in [21], in order to highlight the role of the array baseline lengths (through matrices $\boldsymbol{\Delta}_x$ and $\boldsymbol{\Delta}_y$) in the Fisher information.

A closed-form expression of the stochastic CRB for DOAs has been derived in [20], for instance. In our case, by denoting as $\mathbf{CRB}(l, m)$ the block of the CRB matrix $\mathbf{C_{CR}}$ that pertains to parameters l and m, this expression becomes:

$$\mathbf{CRB}(l, m) = \frac{1 + P\,\mathrm{SNR}}{2NP\,\mathrm{SNR}^2} \operatorname{Re}\Big[\mathbf{D}^\mathsf{H}\boldsymbol{\Pi}_\mathbf{a}^\perp\mathbf{D}\Big]^{-1} \tag{12}$$

where $\boldsymbol{\Pi}_\mathbf{a}^\perp = \mathbf{I} - \frac{1}{P}\mathbf{a}(\boldsymbol{\ell})\,\mathbf{a}^\mathsf{H}(\boldsymbol{\ell})$, and $\mathbf{D} = \frac{\partial \mathbf{a}(\boldsymbol{\ell})}{\partial \boldsymbol{\ell}^\mathsf{T}} = -\mathrm{j}\frac{2\pi}{\lambda}\Big[(\mathbf{x} - \frac{l}{\sqrt{1-l^2-m^2}}\mathbf{z}) \odot \mathbf{a}, (\mathbf{y} - \frac{m}{\sqrt{1-l^2-m^2}}\mathbf{z}) \odot \mathbf{a}\Big]$, in which $\mathbf{x}$, $\mathbf{y}$ and $\mathbf{z}$ denote the vectors $[x_1, \ldots, x_P]^\mathsf{T}$, $[y_1, \ldots, y_P]^\mathsf{T}$ and $[z_1, \ldots, z_P]^\mathsf{T}$ stacking the x-, y- and z-coordinates of the antennas, respectively, and $\odot$ denotes the Hadamard (element-wise) product. Similarly, an expression of the CRB for the source power S, denoted as $\mathrm{CRB}(S)$, can be obtained as $\mathrm{CRB}(S) = \frac{P(P-1)S^2 + 2(P-1)S\sigma^2 + \sigma^2}{NP(P-1)}$.

2.2.2. Hammersley-Chapman-Robbins bound

For the model in the form of (1), it can be shown that the elements of the matrix $\mathbf{B}$ in (5)-(6) are given by

$$B_{ij} = \left(\frac{|\mathbf{R}(\boldsymbol{\theta}_0)|}{|\mathbf{R}(\boldsymbol{\theta}_i)|\,|\mathbf{R}(\boldsymbol{\theta}_j)|\,|\mathbf{R}^{-1}(\boldsymbol{\theta}_i) + \mathbf{R}^{-1}(\boldsymbol{\theta}_j) - \mathbf{R}^{-1}(\boldsymbol{\theta}_0)|}\right)^N, \tag{13}$$

provided the determinant $|\mathbf{R}^{-1}(\boldsymbol{\theta}_i) + \mathbf{R}^{-1}(\boldsymbol{\theta}_j) - \mathbf{R}^{-1}(\boldsymbol{\theta}_0)|$ is not zero [15, 22]. Explicit expressions for the determinants in (13) were obtained in [15] for a similar model, but with a known noise covariance matrix. Following these lines, similar expressions for the determinant and the inverse of $\mathbf{R}(\boldsymbol{\theta})$ can be obtained:

$$|\mathbf{R}(\boldsymbol{\theta})| = \sigma^{2P}(1 + P\,\mathrm{SNR}) \tag{14}$$

with $\mathrm{SNR} = S/\sigma^2$, and

$$\mathbf{R}^{-1}(\boldsymbol{\theta}) = \frac{1}{\sigma^2}\left[\mathbf{I} - \tilde{\mathbf{a}}(\boldsymbol{\theta})\,\tilde{\mathbf{a}}^\mathsf{H}(\boldsymbol{\theta})\right] \tag{15}$$

after defining $\tilde{\mathbf{a}}(\boldsymbol{\theta}) = \sqrt{C}\,\mathbf{a}(\boldsymbol{\ell})$, with $C = \frac{\mathrm{SNR}}{1+P\,\mathrm{SNR}}$. The expression of the third determinant in the denominator of (13) obtained in [15] can also be extended to the present case, and shown to be

$$\begin{aligned} D_{ij}(\boldsymbol{\theta}_0) &= |\mathbf{R}^{-1}(\boldsymbol{\theta}_i) + \mathbf{R}^{-1}(\boldsymbol{\theta}_j) - \mathbf{R}^{-1}(\boldsymbol{\theta}_0)| \\ &= \gamma^P \Big[(1+P\rho_0\,C_0)(1-P\rho_i\,C_i)(1-P\rho_j\,C_j) \\ &\quad + \rho_0\,\rho_i\,(1-P\rho_j\,C_j)\,|\tilde{\mathbf{a}}_0^{\mathsf{H}}\tilde{\mathbf{a}}_i|^2 \\ &\quad + \rho_0\,\rho_j\,(1-P\rho_i\,C_i)\,|\tilde{\mathbf{a}}_0^{\mathsf{H}}\tilde{\mathbf{a}}_j|^2 \\ &\quad - \rho_i\,\rho_j\,(1+P\rho_0\,C_0)\,|\tilde{\mathbf{a}}_i^{\mathsf{H}}\tilde{\mathbf{a}}_j|^2 \\ &\quad + 2\,\mathrm{Re}\Big(\rho_0\,\rho_i\,\rho_j\,(\tilde{\mathbf{a}}_0^{\mathsf{H}}\tilde{\mathbf{a}}_j)(\tilde{\mathbf{a}}_i^{\mathsf{H}}\tilde{\mathbf{a}}_0)(\tilde{\mathbf{a}}_j^{\mathsf{H}}\tilde{\mathbf{a}}_i)\Big)\Big] \end{aligned} \tag{16}$$

where we have used the following definitions:

$$\tilde{\mathbf{a}}_i = \sqrt{C_i}\,\mathbf{a}(\boldsymbol{\ell}_i) \tag{17}$$

$$C_i = \frac{\mathrm{SNR}_i}{1+P\,\mathrm{SNR}_i} = \frac{(S_i/\sigma_i^2)}{1+P\,(S_i/\sigma_i^2)} \tag{18}$$

$$\gamma = \sigma_i^{-2} + \sigma_j^{-2} - \sigma_0^{-2} \tag{19}$$

$$\rho_i = \sigma_i^{-2}/\gamma, \tag{20}$$

and the subscripts i, j, and 0 of an unknown parameter (l, m, S or σ^2) in the expressions above respectively refer to the i-th test point, the j-th test point, and the true value for this parameter. Finally, by plugging (14) and (16) into (13), the elements of $\mathbf{B}$ are obtained as

$$B_{ij} = \left(\frac{\sigma^{2P}(1+P\,\mathrm{SNR})}{\sigma_i^{2P}\sigma_j^{2P}(1+P\,\mathrm{SNR}_i)(1+P\,\mathrm{SNR}_j)\,D_{ij}(\boldsymbol{\theta}_0)}\right)^N, \tag{21}$$

and the Barankin-type bound can be computed using (5).

3. Optimization of antenna placement

3.1. Optimization problem set-up

In this paper, array design is formulated as an antenna selection problem. We do so by defining a set of P candidate antenna locations, and by selecting a subset of M antenna among those P candidates, which minimizes a predefined cost function. In our study, this criterion will be based on either the CRB matrix $\mathbf{C}_{\mathrm{CR}}$, or the BTB matrix $\mathbf{C}_{\mathrm{B}}$. Specifically, we seek to solve the following optimization problem:

$$\begin{aligned} &\min_{\mathbf{w}} \; f(\mathbf{C}(\mathbf{w})) \\ &\text{s.t. } \mathbf{1}^{\mathsf{T}}\mathbf{w} = M \\ &\qquad \mathbf{w} \in \{0,1\}^P \end{aligned} \tag{22}$$

where $\mathbf{w} = [w_1, \ldots, w_P]^{\mathsf{T}}$ denotes the antenna selection vector, i.e., $w_p = 1$ if the pth antenna is selected, and $w_p = 0$ if it is not, and $f(\mathbf{C}(\mathbf{w}))$ is the cost function related to the matrix lower bound $\mathbf{C}(\mathbf{w})$ chosen as selection criterion. Several functions f are possible [23], relating to different types of optimality. In this study, we will use the trace of the matrix bound, i.e., $f(\mathbf{C}(\mathbf{w})) = \mathrm{tr}(\mathbf{C}(\mathbf{w}))$, as it minimizes the total MSE of the unknown parameters. The noise variance σ^2 is assumed to be unknown, but is treated as a nuisance parameter, which means that the matrix $\mathbf{C}(\mathbf{w})$ appearing in the cost function will actually be the (upper-left) 3×3 block of $\mathbf{C}_{\mathrm{CR}}$ or $\mathbf{C}_{\mathrm{B}}$, corresponding to the MSE of the parameters of interest l, m, and S. Finally, the antenna selection problem can be stated as

$$\begin{aligned} &\min_{\mathbf{w}} \; \mathrm{tr}(\boldsymbol{\Psi}\mathbf{C}(\mathbf{w})\boldsymbol{\Psi}^{\mathsf{T}}) \\ &\text{s.t. } \mathbf{1}^{\mathsf{T}}\mathbf{w} = M \\ &\qquad \mathbf{w} \in \{0,1\}^P \end{aligned} \tag{23}$$

where $\boldsymbol{\Psi} = [\mathbf{I}\ \mathbf{0}]$ is the (3×4) matrix which extracts the elements corresponding to the parameters of interest (l, m, S), $\mathbf{C}(\mathbf{w})$ either denotes $\mathbf{C}_{\mathrm{CR}}$ or $\mathbf{C}_{\mathrm{B}}$, and M is the antenna budget (that is the number of selected antennas).

It is generally possible to solve the problem (23) efficiently by using convex relaxation or greedy approaches. However, it is not easy to adapt these methods to the case of a BTB, due to the presence of (possibly many) test points. In this paper, since we aim at comparing the relevance of the CRB-based and the BTB-based criteria for antenna placement, we study a reduced-dimension problem where an exhaustive search method is affordable. Namely, inspiring from existing interferometric antenna array geometries, we consider the case of star-shaped arrays, although it is also possible to apply the described methodology to other (e.g., closed) configurations. We define a maximum aperture $D_{\max}$ for the antenna array, and a number M_B of straight branches, evenly spaced in angle. Each branch contains a number L of uniformly spaced candidate antenna locations. The antenna budget is fixed to $M = M_L\,M_B$, where M_L is the number of selected antenna on a branch. The antenna selection procedure is performed by evaluating the cost function for the whole array with M_B branches, and by carrying out an exhaustive search of the M_L antennas, among the L candidates, that minimize this cost function (all the branches are imposed to be identical).

3.2. Practical computation of the Barankin bound

The test points $\boldsymbol{\theta}_k$ used to compute the Barankin bound can be freely chosen, however they should be selected so as to obtain the tightest bound possible. An approach to do so consists in defining a grid over the parameter space. However, this rapidly becomes unfeasible as the

number of unknown parameters, and thus the number of test points, increase, as the computation of $\mathbf{C}_{\mathrm{B}}$ requires inversion of the $(K \times K)$ matrix $\mathbf{B} - \mathbf{1}\mathbf{1}^{\mathsf{T}}$, where K is the number of test points. In order to reach a trade-off between computation complexity and tightness of the bound, test points can be chosen at sidelobe locations for each unknown parameter. This is particularly useful regarding the source direction (parameters l and m), however there exists no sidelobes for source and noise powers S and σ^2. Consequently, in the sequel, the BTB is computed using 20 test points for (l, m) chosen in $(-1, 1) \times (-1, 1)$ around sidelobes of the array beampattern for each candidate configuration, while 3 test points are used for S and σ^2 in the vicinity of their true values, namely $(0.9, 0.99, 1.1)\, S_0$ and $(0.9, 0.99, 1.1)\, \sigma_0^2$, respectively. It should be noted that these test points are used to evaluate the bound numerically and are intended to span the parameter space. After having performed extensive numerical experiments with different test-point values, we have not noticed any significant variation in the value of the bound, and finally chose these values.

4. Numerical results

In this section, we compare the performance of arrays obtained from the CRB and the BTB in terms of single-source parameter estimation and imaging abilities. We consider the case of an array with $M_B = 3$ straight branches, with $M_L = 7$ antennas on each branch (thus a total of $M = 21$ antennas). We set $D_{\max} = 10\lambda$, and each branch consists in $L = 20$ candidate antenna locations with $\lambda/4$-interspacing. We consider a zenithal observation, i.e., $l = m = 0$, with $N = 100$. It is worth noting that, at high SNR, the BTB coincides with the CRB, so that both criteria are expected to yield equivalent results. At lower SNR, since the BTB reflects the threshold effect, while the CRB does not, both criteria substantially differ, and the BTB seems a more relevant choice. In the following experiments, we set $\mathrm{SNR}_{\mathrm{dB}} = 10 \log_{10} \mathrm{SNR} = -12$ dB.

The results of the proposed antenna selection procedure are presented in Fig. 1. It can be noticed that the CRB-based criterion leads to a configuration where antennas are located at the very ends of the branches. On the other hand, the BTB leads to a somewhat different configuration, with closely-spaced antennas near the array center, and an increasing spacing towards the ends of the branches.

It is instructive to assess an array lay-out in terms of baseline diversity (or completeness of spatial frequency domain sampling), through the so-called *uv*-plane coverage. It corresponds to the collection of the array normalized baseline vectors, i.e., $\mathcal{S}_{\mathbf{u}} = \{\mathbf{u}_{ij} = (\boldsymbol{\xi}_i - \boldsymbol{\xi}_j)/\lambda,\ i, j = 1, \ldots, M\}$, projected on the plane orthogonal to the reference direction (in this case the direction $l = m = 0$). For a single-snapshot zenithal observation, it coincides with the notion of difference coarray that arises in array processing [24]. The *uv*-plane fills up during the observation, as the Earth rotates and the angle with which the array is seen from the source reference direction changes. The *uv*-plane coverage thus provides insight about the imaging capabilities of a radio interferometer as it is linked to the point-spread function of the instrument through a Fourier transform [4], and it determines its ability to capture different angular scales on the sky. Fig. 2 presents the *uv*-plane coverage of arrays obtained from CRB and BTB minimization, for a snapshot observation as well as a for 4-hour observation, where the antennas are assumed to be placed on the surface of the Earth at a latitude of 47°. It can be observed that the BTB-based array has a higher baseline diversity than the CRB-based array, and thus a superior coverage of the *uv*-plane. In Fig. 3, we provide the array beampatterns of both configurations. For an easier comparison, we also plot these beampatterns along the $l = 0$ direction as well as the diagonal ($l = m$) direction. It can be seen that the mainlobe of the BTB-based array is only slightly wider while its sidelobes are considerably lower than those of the CRB-based array.

Then, both arrays are compared in terms of estimation performance for the source parameters (DOA and intensity) according to model (1)–(3) in Figs. 4 and 5. The absolute biases of the MLE for the estimation of l and S were computed by running 10 000 Monte-Carlo simulations, and are shown in Figs. 4(a) and 5(a), respectively. The MSE of the MLE (also obtained from Monte-Carlo simulations) and the corresponding CRB and BTB for the estimation of l and S are shown in Figs. 4(b) and 5(b), respectively. Results regarding estimation of m are identical to those for l, and are consequently not shown here. Regarding DOA estimation (Fig. 4), the behavior of the BTB reflects that of the MSE fairly well, with a difference of about 7 dB between the SNR threshold predicted by the BTB and that of the MLE, for the BTB-based array. Most importantly, the threshold SNR for the BTB-based array is about 5 dB below that of the CRB-based array, leading to a significantly lower MSE over a wide SNR range (from -11 dB to -5 dB) for the BTB-based array. The accuracy gained in this SNR range comes at the expense of asymptotic accuracy, as the CRB for the CRB-based array is slightly lower than that of the BTB-based array (which is related to the difference in the main-lobe width noticed in Fig. 3). On the other hand, it is seen from Fig. 5 that the estimation

performance of both arrays regarding the source intensity S is essentially the same. We conclude that the BTB seems more suitable than the CRB for array design, as it leads to an array that yields superior source parameter estimation performance in this regime.

These results clearly illustrate how the CRB and the BTB lead to different array configurations. To a fairly large extent, these results can be effectively explained from known results in array processing. In particular, it was shown in [22] that the CRB for the DOA of a single source, which relates to small estimation errors, is linked to the second derivative of the array beampattern at the origin, that is its curvature. Consequently, a CRB-based design criterion only focuses on the thinness of the mainlobe, and thus systematically results in an array with a maximal aperture, at the expense of the sidelobe level. It can also be seen from (9) and (10) that long baselines imply large values in matrices $\mathbf{\Delta}_x$ and $\mathbf{\Delta}_y$ arising in the FIM, hence contributing to minimize the CRB. In contrast, the BTB-based criterion yields a configuration with less antennas concentrated at the edges, and thus a synthesized beam with lower sidelobes. It is also worth noting that assuming the source intensity S is unknown does not affect the SNR threshold value on the DOA estimation, compared with a situation where S would be known [25].

Finally, we assess the performance of both array geometries in terms of imaging accuracy, as can be done in radio astronomy. In this case, the antenna arrays receive signals from more than a single source. Although the single-source assumption used to derive our design criteria does not actually hold in this case, it is insightful to assess the imaging capability of the obtained geometries. A test image of the M51 galaxy, that is assumed to represent the true source structure, is given in Fig. 6(a). An imaging algorithm, based on an Expectation-Maximization (EM) approach including sparsity constraints [26], is applied to obtain images for both CRB- and BTB-based arrays. These images are computed in a realistic radio-astronomy scenario, where the antennas are assumed to be placed on the surface of the Earth, with the array center at a latitude of 47°, and taking Earth rotation into account. As usually done in radio interferometry, the imaging method makes use of visibility data that correspond to the correlations of the antenna signals, obtained as $\widehat{\mathbf{R}}_i = \frac{1}{N}\sum_{n=(i-1)N}^{iN-1} \mathbf{y}_n\mathbf{y}_n^{\mathsf{H}}$, $i = 1, \ldots, N_{\text{snapshot}}$, averaged over N antenna signal samples. The obtained images for the CRB-based and the BTB-based array are provided in Figs. 6(b) and 6(c), for a 4-hour observation time, using $N_{\text{snapshot}} = 48$ snapshots, obtained by averaging $N = 5 \cdot 10^5$ antenna signal samples, which corresponds to $N_{\text{vis}} = N_{\text{snapshot}}\, M^2 = 21\,168$ visibilities. Finally, we report in Table 1 the normalized MSE (NMSE) for the same image reconstruction set-up, averaged over 100 noise realizations. The NMSE metric is defined by

$$\text{NMSE} = \frac{\sum_{i,j}|S_{0,ij} - \widehat{S}_{ij}|^2}{\sum_{i,j}|S_{0,ij}|^2} \tag{24}$$

where $S_{0,ij}$ is the true (i, j)-pixel intensity and $\widehat{S}_{ij}$ is the estimated (i, j)-pixel intensity. It can be seen that the BTB-based array performs markedly better in terms of imaging accuracy than the CRB-based one. These results confirm that the BTB-based array design criterion is more suitable than that based on the CRB for an imaging purpose. The fact that the BTB allows to handle the sidelobe level, as explained above, translates into less ambiguities than the CRB criterion in the reconstructed images, as can be seen from Fig. 6. Of course, this in no way implies that the proposed BTB-based design criterion is optimal for imaging. From Fig. 2, it can be seen that there is a range of spatial frequencies which are not sampled, resulting in a ring-shaped hole in the *uv*-domain for a synthesis observation. The single-source model used does of course not fully grasp the complexity of the imaging problem, but the results in terms of imaging argue in favor of a BTB-type design criterion. In the end, it can be viewed as a criterion based on the expected performance of image reconstruction algorithms, and may be considered for the selection of a radio-interferometer configuration. The CRB may still prove relevant for array design, but would require the use of more sophisticated models (with more than a single source) to obtain geometries that mitigate the sidelobe level in the array beampattern.

5. Conclusions

In this article, we have compared two antenna selection approaches, respectively based on the CRB and a BTB. The performance of both optimized array geometries has been evaluated based on several criteria relevant to parameter estimation, such as a source's DOA and intensity, and to radio-interferometric imaging applications, such as the *uv*-plane coverage, the array beampattern and the recovery of a more complex radio source structure. Simulation results demonstrate that a design criterion based on the BTB leads to an optimal trade-off (in the MSE sense) between the array's main-lobe width and sidelobe level, resulting in (i) a lower overall MSE for the parameters of a point source over a fairly wide range of (moderate) SNR, and (ii) an enhanced imaging capability of the array compared with a CRB-based design criterion.

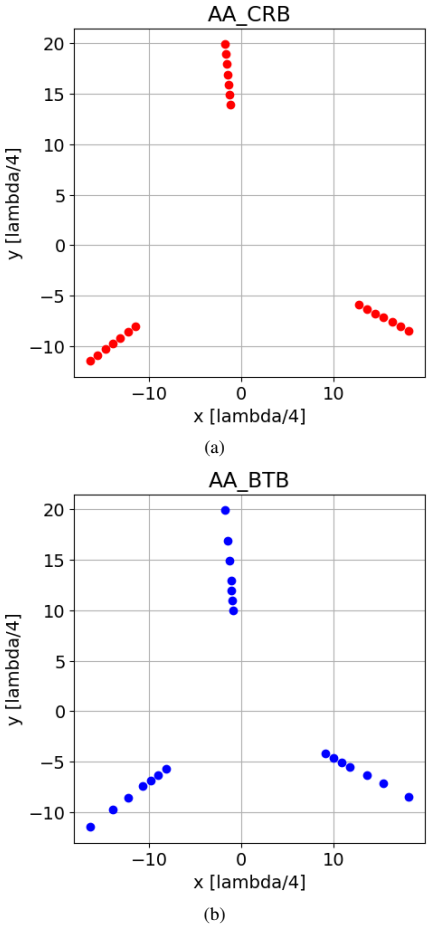

Figure 1: Antenna array obtained from (a) the CRB-based criterion, (b) the BTB-based criterion.

Table 1: NMSEs for M51 image reconstruction using CRB-based and BTB-based arrays, obtained after averaging over 100 Monte-Carlo trials (standard deviations are indicated between brackets).

	NMSE
CRB array	0.33 (±0.005)
BTB array	0.09 (±0.005)

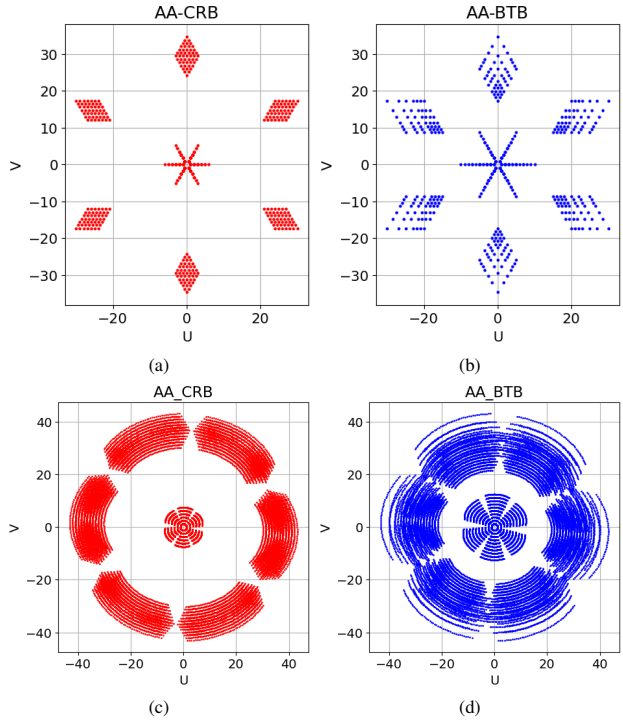

Figure 2: Coverage of the *uv*-plane obtained for a snapshot observation (a)-(b) and for a 4-hour observation (c)-(d), for the CRB-based array (on the left: (a) and (c)), and the BTB-based array (on the right: (b) and (d)).

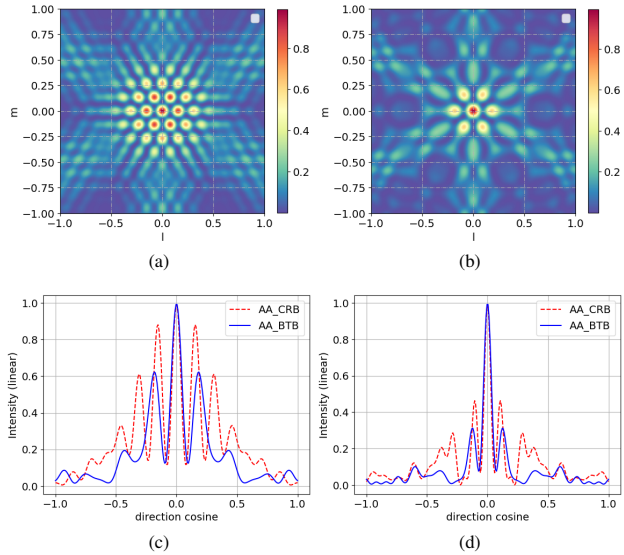

Figure 3: Array beampatterns of the CRB-based array (a) and the BTB-based array (b), 1D-comparison of both along the $l = 0$ direction (c) and along the diagonal ($l = m$) direction (d).

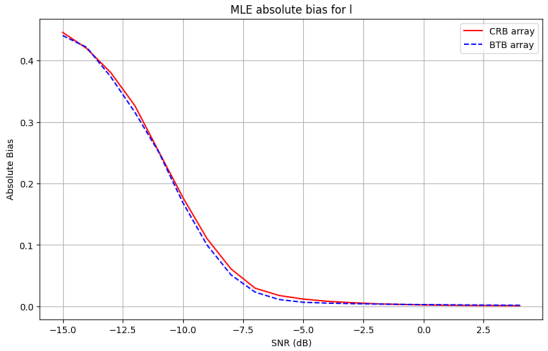

(a)

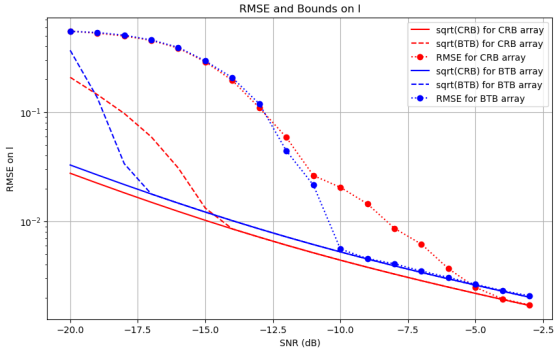

(b)

Figure 4: Comparison of the estimation performance of direction cosine l: (a) absolute bias of the MLE for both CRB-based and BTB-based array geometries, and (b) square roots of the CRBs and BTBs, and RMSEs, for both arrays. Red curves regard the CRB-based array, while blue curves regard the BTB-based array. In (b), solid lines, dashed lines, and solid lines with point markers respectively represent the (square roots of the) CRBs and BTBs, and RMSEs.

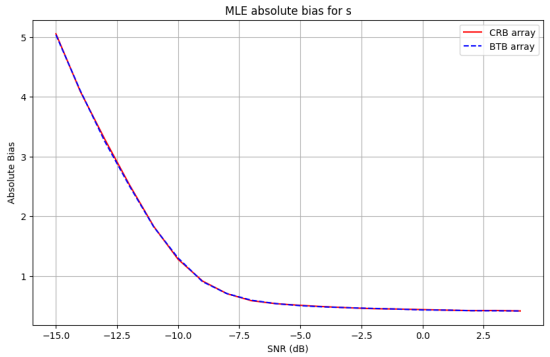

(a)

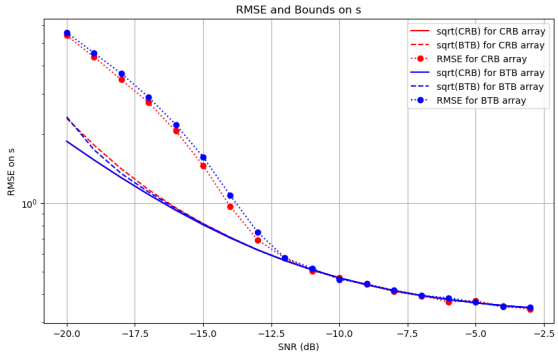

(b)

Figure 5: Comparison of the estimation performance of direction cosine S: (a) absolute bias of the MLE for both CRB-based and BTB-based array geometries, and (b) square roots of the CRBs and BTBs, and RMSEs, for both arrays. Red curves regard the CRB-based array, while blue curves regard the BTB-based array. In (b), solid lines, dashed lines, and solid lines with point markers respectively represent the (square roots of the) CRBs and BTBs, and RMSEs.

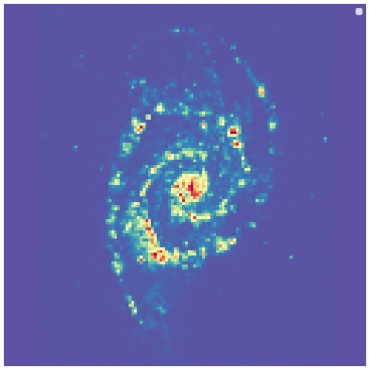

(a)

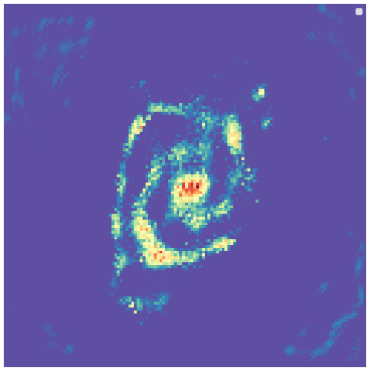

(b)

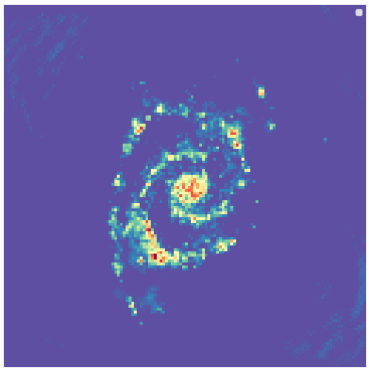

(c)

Figure 6: Image of the M51 galaxy used as sky model (true image, with size 128×128) (a), and imaging results for the CRB-based array (b) and the BTB-based array (c).

References

[1] M. P. van Haarlem et al., LOFAR: The LOw Frequency ARray, Astronomy and Astrophysics 556 (2013) A2.

[2] M. G. Labate, M. Waterson, B. Alachkar, A. Hendre, P. Lewis, M. Bartolini, P. Dewdney, Highlights of the Square Kilometre Array Low Frequency (SKA-LOW) Telescope, Journal of Astronomical Telescopes, Instruments, and Systems 8 (2022) 011024.

[3] G. P. Swart, P. E. Dewdney, A. Cremonini, Highlights of the SKA1-Mid telescope architecture, Journal of Astronomical Telescopes, Instruments, and Systems 8 (2022) 011021.

[4] A. R. Thompson, J. M. Moran, G. W. Swenson, Interferometry and Synthesis in Radio Astronomy, 3rd Edition, Astronomy and Astrophysics Library, Springer International Publishing, Cham, 2017.

[5] E. Keto, The shapes of cross-correlation interferometers, The Astrophysical Journal 475 (2) (1997) 843–852.

[6] F. Boone, Interferometric array design: Optimizing the locations of the antenna pads, Astronomy and Astrophysics 377 (1) (2001) 368–376.

[7] V. Ollier, M. N. El Korso, A. Ferrari, R. Boyer, P. Larzabal, Robust distributed calibration of radio interferometers with direction dependent distortions, Signal Processing 153 (2018) 348–354.

[8] J.-P. Delmas, M. N. El Korso, H. Gazzah, M. Castella, CRB analysis of planar antenna arrays for optimizing near-field source localization, Signal Processing 127 (2016) 117–134.

[9] M. Juhlin, A. Jakobsson, Optimal sensor placement for localizing structured signal sources, Signal Processing 202 (2023) 108679.

[10] K. Todros, J. Tabrikian, General classes of performance lower bounds for parameter estimation – Part I: non-Bayesian bounds for unbiased estimators, IEEE Transactions on Information Theory 56 (10) (2010) 5045–5063.

[11] E. Chaumette, A. Renaux, M. N. El Korso, A class of Weiss-Weinstein bounds and its relationship with the Bobrovsky-Mayer-Wolf-Zakaï bounds, IEEE Transactions on Information Theory 63 (4) (2017) 2226–2240.

[12] D. G. Chapman, H. Robbins, Minimum variance estimation without regularity assumptions, Annals of Mathematical Statistics 22 (4) (1951) 581–586.

[13] E. W. Barankin, Locally best unbiased estimates, Annals of Mathematical Statistics 20 (4) (1949) 477–501.

[14] I. Reuven, H. Messer, The use of the Barankin bound for determining the threshold SNR in estimating the bearing of a source in the presence of another, in: Proc. of IEEE International Conference on Acoustics, Speech, and Signal Processing (ICASSP), Vol. 3, Detroit, MI, USA, 1995, pp. 1645–1648.

[15] J. Tabrikian, J. L. Krolik, Barankin bounds for source localization in an uncertain ocean environment, IEEE Transactions on Signal Processing 47 (11) (1999) 2917–2927.

[16] O. Aharon, J. Tabrikian, A simple and tight Bayesian lower bound for direction-of-arrival estimation, in: Proc. of IEEE Workshop on Statistical Signal Processing (SSP), Hanoi, Vietnam, 2023, pp. 26–30. doi:10.1109/SSP53291.2023.10207970.

[17] J. Tabrikian, O. Isaacs, I. Bilik, Cognitive antenna selection for automotive radar using Bobrovsky-Zakai bound, IEEE Journal on Selected Topics in Signal Processing 15 (4) (2021) 892–903.

[18] B. Ottersten, M. Viberg, P. Stoica, A. Nehorai, Exact and large sample maximum likelihood techniques for parameter estimation and detection in array processing, in: S. Haykin, J. Litva, T. J. Shepherd (Eds.), Radar Array Processing, Springer Berlin Heidelberg, Berlin, Heidelberg, 1993, Ch. 4, pp. 99–151.

[19] P. Stoica, B. Ottersten, M. Viberg, R. L. Moses, Maximum likelihood array processing for stochastic coherent sources, IEEE Transactions on Signal Processing 44 (1) (1996) 96–105.

[20] P. Stoica, E. G. Larsson, A. B. Gershman, The stochastic CRB for

array processing: a textbook derivation, IEEE Signal Processing Letters 8 (5) (2001) 148–150.
[21] S. J. Wijnholds, A.-J. van der Veen, Fundamental imaging limits of radio telescope arrays, IEEE Journal on Selected Topics in Signal Processing 2 (5) (2008) 613–623.
[22] H. Messer, Source localization performance and the array beampattern, Signal Processing 28 (2) (1992) 163–181.
[23] S. P. Chepuri, G. Leus, Sparsity-promoting sensor selection for nonlinear measurement models, IEEE Transactions on Signal Processing 63 (3) (2015) 684–698.
[24] R. T. Hoctor, S. A. Kassam, The unifying role of the coarray in aperture synthesis for coherent and incoherent imaging, Proceedings of the IEEE 78 (4) (1990) 735–752.
[25] I. Reuven, H. Messer, On the effect of nuisance parameters on the threshold SNR value of the Barankin bound, IEEE Transactions on Signal Processing 47 (2) (1999) 523–527.
[26] Y. Mhiri, M. N. El Korso, A. Breloy, P. Larzabal, A robust EM algorithm for radio interferometric imaging in the presence of outliers, in: IEEE Workshop on Signal Processing Systems (SiPS), Rennes, France, 2022, pp. 1–5.